



**Results from E735 at the Tevatron
Proton-Antiproton Collider with $\sqrt{s} = 1.8$ TeV**

C. Lindsey

*Fermi National Accelerator Laboratory
P.O. Box 500, Batavia, Illinois 60510*

November 1991

* Presented at the *Quark Matter 1991*, Gatlinberg, Tennessee, November 11-15, 1991.



Disclaimer

This report was prepared as an account of work sponsored by an agency of the United States Government. Neither the United States Government nor any agency thereof, nor any of their employees, makes any warranty, express or implied, or assumes any legal liability or responsibility for the accuracy, completeness, or usefulness of any information, apparatus, product, or process disclosed, or represents that its use would not infringe privately owned rights. Reference herein to any specific commercial product, process, or service by trade name, trademark, manufacturer, or otherwise, does not necessarily constitute or imply its endorsement, recommendation, or favoring by the United States Government or any agency thereof. The views and opinions of authors expressed herein do not necessarily state or reflect those of the United States Government or any agency thereof.

RESULTS FROM E735 AT THE TEVATRON PROTON-ANTIPROTON COLLIDER WITH $\sqrt{s} = 1.8$ TeV*

Clark S. Lindsey

Fermilab, P.O. Box 500, Batavia, Illinois 60510, U.S.A.

For the E735 Collaboration:

T. Alexopoulos⁽⁷⁾, C. Allen⁽⁶⁾, E.W. Anderson⁽⁴⁾, V. Balamurali⁽⁵⁾, S. Banerjee⁽⁵⁾, P.D. Beery⁽⁵⁾, P. Bhat⁽³⁾, N.N. Biswas⁽⁵⁾, A. Bujak⁽⁶⁾, D.D. Carmony⁽⁶⁾, T. Carter⁽²⁾, P. Cole⁽⁶⁾, Y. Choi⁽⁶⁾, R. DeBonte⁽⁶⁾, V. DeCarlo⁽¹⁾, A.R. Erwin⁽⁷⁾, C. Findeisen⁽⁷⁾, A.T. Goshaw⁽²⁾, L.J. Gutay⁽⁶⁾, A.S. Hirsch⁽⁶⁾, C. Hojvat⁽³⁾, J.R. Jennings⁽⁷⁾, V.P. Kenny⁽⁵⁾, C.S. Lindsey⁽³⁾, C. Loomis⁽²⁾, J.M. LoSecco⁽⁵⁾, T. McMahon⁽⁶⁾, A.P. McManus⁽⁵⁾, N. Morgan⁽⁶⁾, K. Nelson⁽⁷⁾, S.H. Oh⁽²⁾, N.T. Porile⁽⁶⁾, D. Reeves⁽³⁾, A. Rimai⁽⁶⁾, W.J. Robertson⁽²⁾, R.P. Scharenberg⁽⁶⁾, B.C. Stringfellow⁽⁶⁾, S.R. Stampke⁽⁵⁾, M. Thompson⁽⁷⁾, F. Turkot⁽³⁾, W.D. Walker⁽²⁾, C.H. Wang⁽⁴⁾, J. Warchol⁽⁵⁾, D.K. Wesson⁽³⁾, Y. Zhan⁽⁵⁾

(1) Department of Physics, DePauw University, Greencastle, IN 46135

(2) Department of Physics, Duke University, Durham, NC 22706

(3) Fermi National Accelerator Laboratory P.O. Box 500, Batavia, IL 60510

(4) Department of Physics, Iowa State University, Ames, IA 50011

(5) Department of Physics, University of Notre Dame, Notre Dame, IN 46556

(6) Department of Physics and Chemistry, Purdue University, W. Lafayette, IN 47907

(7) Department of Physics, University of Wisconsin, Madison, WI 53706

Abstract

Experiment E735[†] searched for evidence of the transition to quark-gluon plasma in $p\bar{p}$ collisions at $\sqrt{s} = 1.8$ TeV. Using data from a high statistics run in 1988-1989, results are presented on multiplicity distributions, hyperon and phi production, and Bose-Einstein correlations. Some data was also taken at lower collision energies and results will be compared to previous experiments.

1. INTRODUCTION

Experiment E735 studied minimum trigger bias $p\bar{p}$ collisions at the Tevatron collider at Fermilab. The primary goal was the search for evidence of the transition from normal hadronic matter to the quark-gluon plasma phase (QGP). The transition is expected to occur at very high energy densities. Energy density can be related to the charged

*Plenary talk at Quark Matter '91, Ninth Int. Conf. on Ultra-Relativistic Nucleus-Nucleus Collisions, Gatlinburg, Tennessee, Nov. 11-15, 1991.

[†]This work was performed at the Fermi National Accelerator Laboratory, which is operated by the Universities Research Association, Inc., contract DE-AC02-76CHO3000 with the U.S. Dept. of Energy.

multiplicity of the collision by the formula¹:

$$\epsilon = \frac{3}{2} \frac{dN_c}{d\eta} \frac{(\langle p_{\perp} \rangle^2 + m_{\pi}^2)^{1/2}}{\tau \pi r^2},$$

where τ and r are the interaction time and transverse radius of the collision fireball, respectively. Plotting measured quantities such as $\langle p_{\perp} \rangle$ or strangeness production versus charge multiplicity might show dramatic changes as the energy density increases with increasing multiplicity if a QGP transition occurred. For example, it was speculated that the flattening in $\langle p_{\perp} \rangle$ versus $dN_c/d\eta$ at high multiplicity seen by UA1, where $\langle p_{\perp} \rangle$ can be related to the temperature in the fireball, could indicate the onset of a mixed phase.²

In previous reports we have presented as a function of the charged particle multiplicity: the $\langle p_{\perp} \rangle$ for all charge particles and for pions, kaons and protons and the relative production to pions of kaons, and protons.³⁻⁶ Here, we will present some preliminary results from a high statistics run on measurements of the charged multiplicity itself, and on hyperon production, phi production and Bose-Einstein correlations and their dependence on multiplicity.

2. EXPERIMENT E735

The E735 system of detectors has been described in detail elsewhere (see references 7-12). Figure 1 shows a plan view of the E735 detectors. The system is divided into roughly two parts: the interaction hall detectors and the spectrometer. The interaction hall detectors surrounded the collision point. They consisted of a vertex chamber,⁷ the central tracking chamber (CTC),⁸ the hodoscope array of scintillators,⁹ and two arrays of time of flight (TOF) counters.¹⁰ These central detectors served primarily to count the number of charged particles in the events and to determine the trigger. The spectrometer sampled charged tracks from the central region to determine their momenta and particle identification.

The arrays of time of flight trigger counters in the upstream and downstream regions (relative to the proton direction) used the hit times of the fastest particles to determine both the interaction time and the event vertex along the beam line. The TOF trigger arrays consisted of 15 counters each and covered pseudo-rapidity range of $3 < |\eta| < 4.5$. The online trigger required one or more hits in both trigger arrays in coincidence with the beam crossing. A vertex chamber, located 14 cm from the beam line, also provided the event vertex along the beam line with a r.m.s. resolution of 2.5 cm.

The 240 counters of the hodoscope array covered $|\eta| < 3.25$. In figure 1 can be seen the three sections of the hodoscope: the *barrel* and the two *endcap* hodoscopes. There were 96 counters covering $|\eta| < 1.62$ in the barrel that surrounded the CTC, with 48 counters in each positive and negative rapidity region. The endcap hodoscopes covered $1.62 < |\eta| < 3.25$ in the forward and backward directions and each had 72 counters. These 72 counters were comprised of 3 rings of 24 counters, each ring spanning 0.5 units of pseudo-rapidity.

The hodoscope scintillators were instrumented for both pulse height and timing measurements. The number of scintillator hits gave a fast indication of the event multiplicity and provided the trigger system the option of scaling the events written to tape according

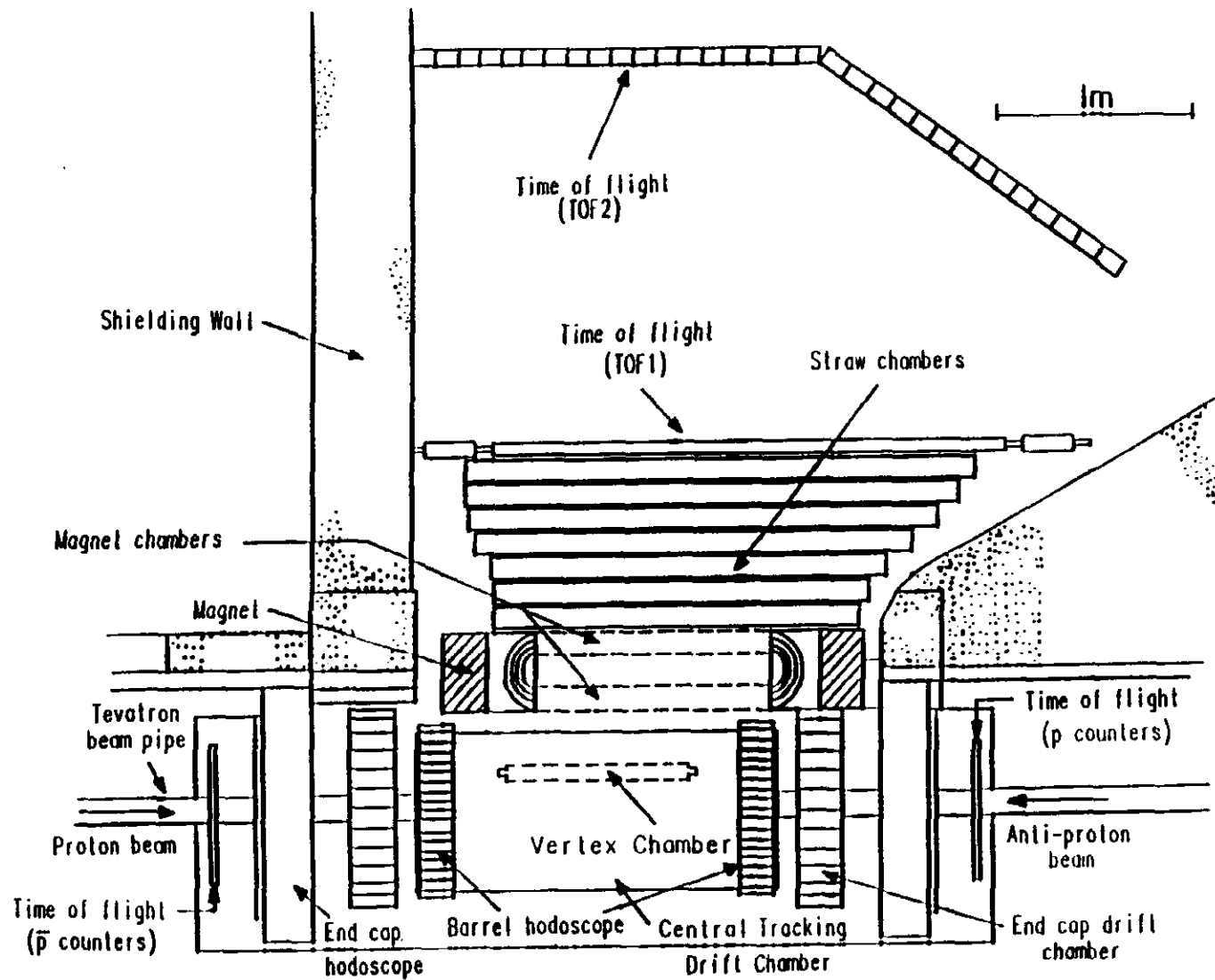


Figure 1 Plan view of experiment E735 at the C0-intersection region.

to multiplicity.¹¹ Most data was taken with lower multiplicity events scaled down in favor of high multiplicity events. Events can later be weighted according to the scale factor for the N_{hodo} hits in the event to obtain distributions that would be found without trigger scaling. (Runs without trigger scaling were used for the multiplicity analysis)

A central tracking chamber measured charged tracks over $|\eta| < 1.7$. The CTC was a cylindrical drift chamber 2 m long and covered a radius from 25 to 38 cm. It was constructed of low-mass carbon fiber-epoxy composite material (0.014 interaction lengths in radial direction) to reduce production of secondaries. There were 24-layer 'jet' type drift cells, each having 24 sense wires. Signals from both ends of the sense wires were sent to flash analog-to-digital converters (FADC). Due to the longer readout time of the CTC signal digitization, about 10 events with only hodoscope information were written to tape for every event with the CTC. So the amount of data with CTC information is much less than that with only hodoscope signals.

The spectrometer arm covers approximately the pseudo-rapidity range $-0.36 < \eta < 1.0$ with an azimuthal angular acceptance of 18 degrees and it includes a dipole magnet with a 50 MeV/c transverse momentum kick. The solid angle of the spectrometer arm is about 0.06 sr. Particle trajectory is measured by three planes of vertex chamber, four planes of *pre-magnet* and four planes of *post-magnet* drift chambers within the magnet aperture. These planes are followed by 14 straw tube drift chamber planes,¹² 6 of which are inclined by 4° for stereo reconstruction. Behind the straw chambers, there are two sets of scintillators at 200 cm and 400 cm from the beam line to measure the time of flight (TOF) of particles in the spectrometer arm. The first set (TOF1) consists of seven 300 cm long horizontal scintillators. The second set (TOF2) consists of thirty two 150 cm long vertical scintillators. Each scintillator is equipped with two phototubes, one at each end of the scintillator. Both charge and time are read out as in the case of the multiplicity hodoscope. The measured charge is used to correct the measured time as a function of charge to avoid time slewing.

There were two runs with the E735 system in the C0 interaction region of the Tevatron collider. A short run in 1987 provided about 5 million triggers to tape. The CTC was not installed and only half of the TOF2 counters were installed. A second longer run occurred in 1988/89 with all detectors installed and about 20 million triggers were written to tape. Because of higher luminosity, during the second run the trigger processor provided a higher percentage of high multiplicity events on tape than during the first run. In the second run there was also data taken at lower energies: $\sqrt{s} = 300$ GeV, 546 GeV, and 1000 GeV.

3. CHARGED MULTIPLICITY

The charged multiplicity was measured by both the CTC and the hodoscope. However, here only the hodoscope multiplicities will be shown. The CTC data is still under study but preliminary results show consistency between the CTC and hodoscope multiplicity. The 240 hodoscope scintillators provided a somewhat coarse measurement of the multiplicity since individual tracks are not observed. Scintillator hits can be caused not only by primary charged particles, but also by decay products of primaries and by particles from secondary interactions in intervening materials. Because of the large amount of data with only hodoscope information, however, it was important to obtain an accu-

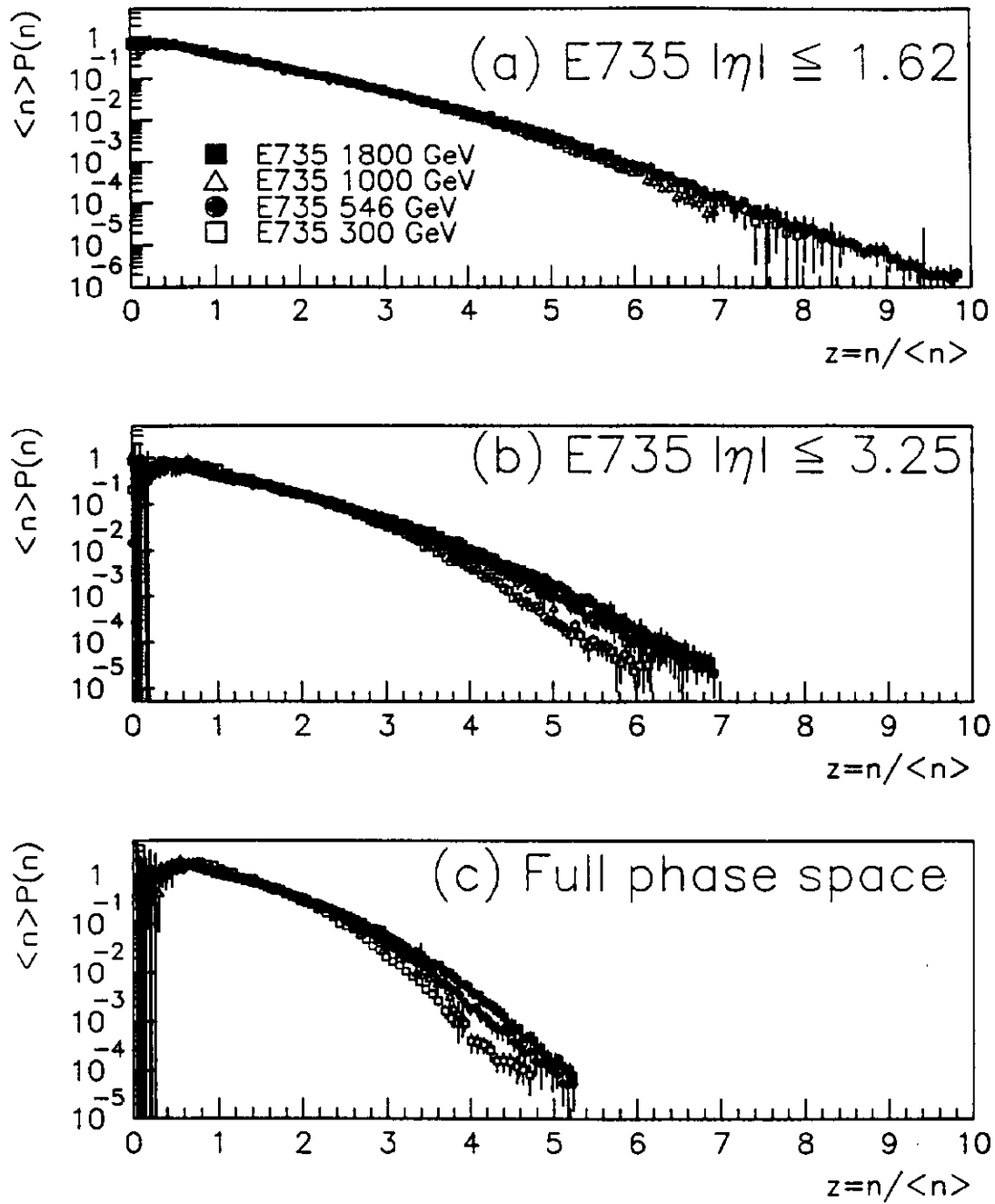


Figure 2. Multiplicity distributions for (a) $|\eta| < 1.62$ in KNO format for four energies; (b) $|\eta| < 3.25$; and (c) full phase space.

rate measure of the charged multiplicity from the hodoscope. To convert the number of hodoscope hits N_{hodo} to N_c primary charged tracks, the following procedure was carried out:

- Generate a $p\bar{p}$ event with the UA5 GENCL event generator¹³ or the Pythia Lund based minimum bias event generator.¹⁴
- Process the event through the Geant detector simulation.¹⁵
- Do trigger and analysis cuts on Monte Carlo data as was done on real data and obtain the trigger acceptance $\epsilon(m)$ function and conversion matrix P_{mn} for the probability of n primary tracks producing m hodoscope hits.
- Unfold the $N_c(n)$ distribution from the $O(m)$ distribution of hodoscope hits directly from

$$N_c(n) = \sum_{m=1}^M P_{mn} O(m) / \epsilon(m)$$

or using the maximum entropy method described in reference 16.

The primary $N_c(n)$ distribution into the pseudo-rapidity range $|\eta| < 1.62$ was obtained from the number of hits in the barrel hodoscope, into $|\eta| < 3.25$ from the full hodoscope, and into full phase space also from the full hodoscope. The dependence of the results, especially for full phase space, on the event generator is still under study.

The UA1 and UA5 experiments at the CERN $p\bar{p}$ Collider studied charged multiplicities at 200 GeV, 546 GeV and 900 GeV energies.¹⁷⁻¹⁹ UA5 found that KNO scaling was violated in full phase space but held for more narrow pseudo-rapidity intervals. UA1 only reported on the $|\eta| < 2.5$ interval and smaller and claimed that KNO scaling held. The negative binomial gave satisfactory fits to the $N_c(n)$ distributions at 200 GeV and 546 GeV but for full phase space only a sum of two negative binomials gave a good fit.²⁰

Figure 2 shows charge multiplicity distributions in KNO format as derived from the hodoscope for the three pseudo-rapidity intervals and for the four center of mass energies. For the $|\eta| < 1.6$ the distributions overlap within errors over the full range of $z = n / \langle n \rangle$ and so obey KNO scaling. The distributions for $|\eta| < 3.25$ and for full phase space do not overlap over the full range, indicating violation of KNO scaling. This is consistent with the UA5 and UA1 results.

Figure 3a shows the multiplicity distribution for 1800 GeV with a fit to a negative binomial.²¹ The negative binomial does not give a good fit. Figure 3b shows that using a sum of two negative binomials, each with independent \bar{N} and k parameters

$$F = wF_1(\bar{N}_1, k_1) + (1 + w)F_2(\bar{N}_2, k_2),$$

a good fit is obtained (also shown are the two functions). This is similar to that reported for the 900 GeV UA5 distributions (see ref. 20). It isn't known, however, whether this really indicates the presence of two components in the interactions (e.g. a KNO scaling component + KNO violating component from mini-jets) or whether the improved fit is simply due to the increase in the number of parameters in the fitting function from 2 to 5.

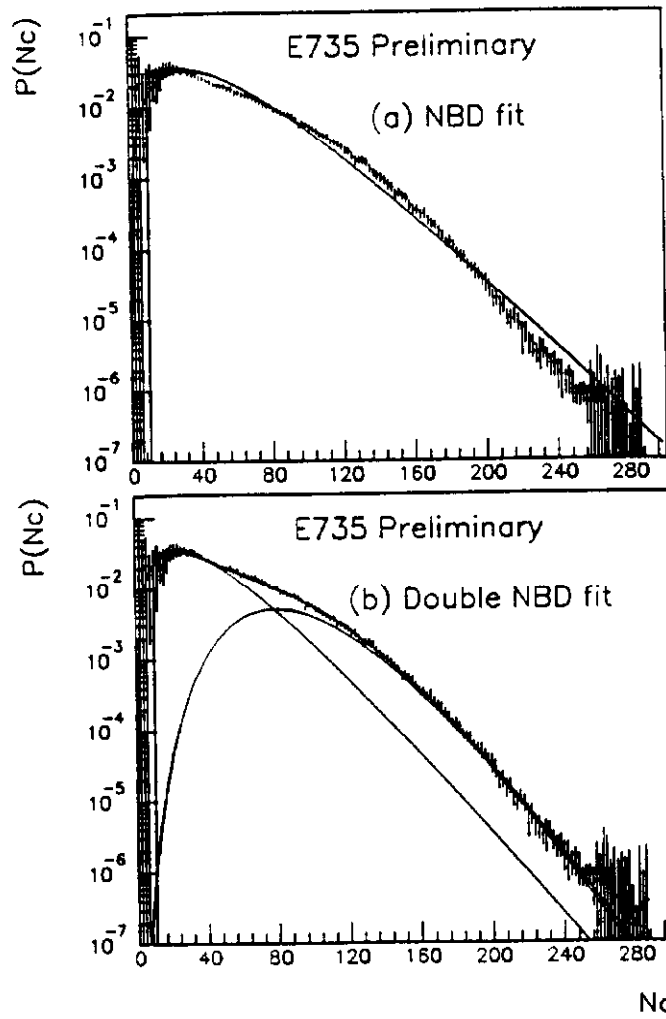


Figure 3.(a) N_c distribution in full phase space at 1800GeV fit to a negative binomial distribution. (b) Fit to a sum of 2 NBD: $F = wF_1(\bar{N}_1, k_1) + (1 + w)F_2(\bar{N}_2, k_2)$ (ref.21).

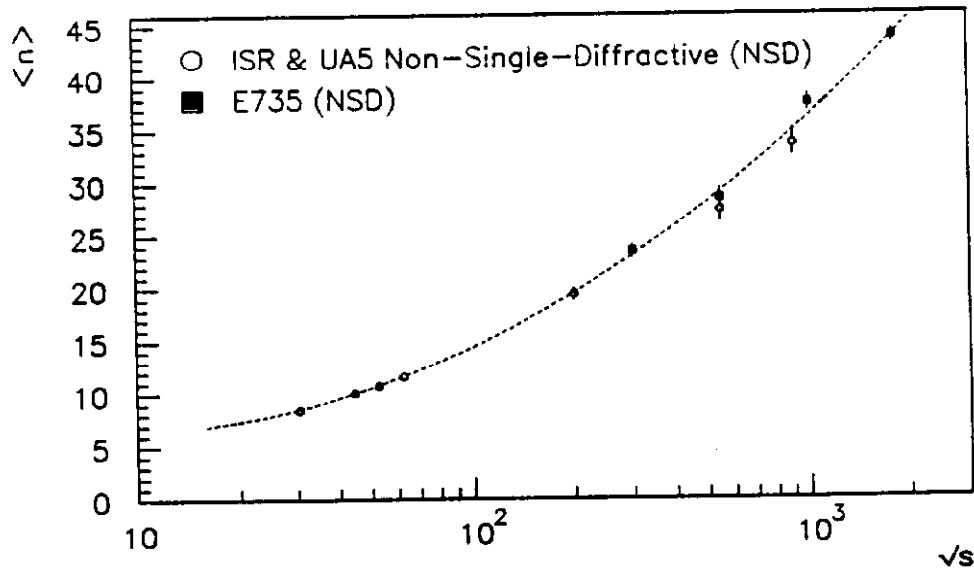


Figure 4. $\langle N_c \rangle$ vs \sqrt{s} for non-single diffractive data from ISR, UA5 and E735.

Figure 4 shows the mean multiplicity as a function of \sqrt{s} for non-single diffractive collisions for full phase space. The curve is a fit to the function $P_1 + P_2 \log(s) + P_3 \log^2(s)$. The E735 mean multiplicities tend to be somewhat larger at the lower energies than the UA5 points but are consistent within errors. Systematic errors in the E735 multiplicity measurements are still under study.

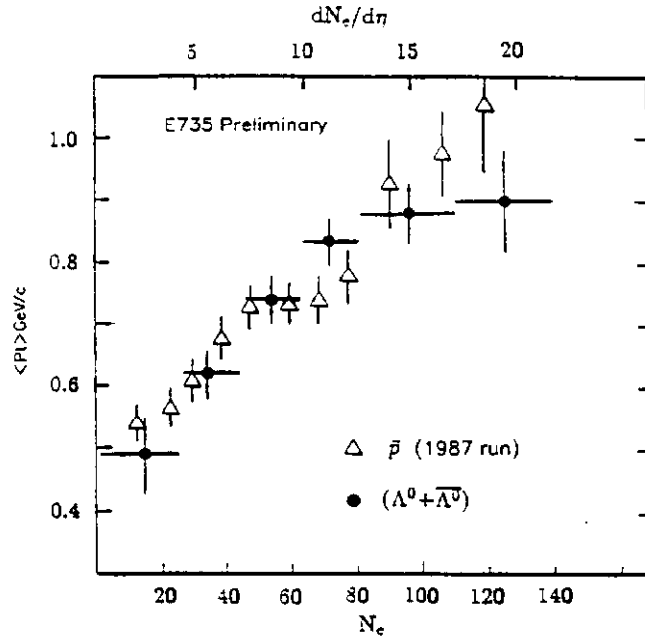


Figure 5. $\langle p_{\perp} \rangle$ versus multiplicity for lambdas and anti-protons.

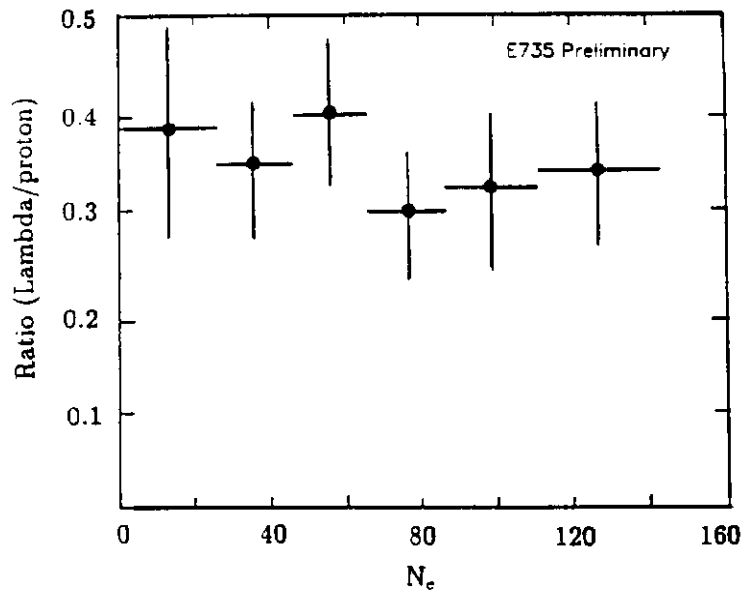


Figure 6. Ratio of lambdas to protons versus multiplicity.

4. Λ^0 and Ξ^- PRODUCTION

An analysis of lambda production has been carried out using the high statistics of the second run.²² Following similar analysis techniques as described in reference 4, about 7000 Λ^0 and $\bar{\Lambda}^0$ above background were found (compared to about 400 in the earlier analysis).

Figure 5 shows the average transverse momentum of lambdas versus multiplicity. (Here and in following figures, the multiplicity is defined as the number of charged particles into $|\eta| < 3.25$ from the hodoscope; divide by 6.50 to obtain $dN_c/d\eta$.) Also, shown is data for anti-protons from reference 5. The $\langle p_\perp \rangle$ increases at about the same rate for each. Figure 6 shows the ratio of lambdas to protons versus multiplicity. The ratio is flat within errors.

In events with $p\pi^-\pi^-$ ($\bar{p}\pi^+\pi^+$) and one of the $p\pi^-$ ($\bar{p}\pi^+$) pairs having invariant mass in the range of the lambda (anti-lambda) cut,

$$1.10\text{GeV}/c^2 < M(p\pi) < 1.13\text{GeV}/c^2,$$

the invariant mass distribution is found to have a peak above background at the cascade mass. After background was subtracted there were about 250 cascades ($\Xi^- + \bar{\Xi}^-$).

With so few cascades it is difficult to determine the average transverse momentum from a distribution of dN/dp_\perp because of the poor statistics. Instead another technique was used. In the invariant mass distributions of $M(p\pi)$ it was noticed that there was a slight excess above the lambda mass. These entries originated from cascade decays,

$$\Xi^- \rightarrow \Lambda^0 \pi_1^-, \quad \Lambda^0 \rightarrow p\pi_2^-,$$

where the proton from the lambda decay is combined with the π_1^- from the Ξ^- decay instead of the π_2^- from the lambda decay. A similar process holds for the anti-cascades. There were about 580 such "wrong paired" lambdas found. The ratio of the wrong paired lambdas to the number of cascades found is proportional to the cascade average p_\perp . This can be seen as due to the fact that if p_\perp is large, more of the cascade three prongs will enter the spectrometer, whereas if p_\perp is small, it is more likely that only two of the three prongs will be seen in the spectrometer. Using a Monte Carlo, a relationship was determined between this ratio and p_\perp . Using this relationship, the cascade p_\perp was determined to be $0.90^{+0.35}_{-0.22}\text{GeV}/c$.

The overall ratio of lambdas to protons is 0.39 ± 0.05 . The ratio of cascades to lambdas is found to be 0.16 ± 0.03 . Using values from reference 5 for the ratios of protons to pions and kaons to pions, we obtain a ratio of 0.026 ± 0.003 for lambdas to all charged particles and a ratio of 0.0042 ± 0.0009 for cascades to all charged particles.

5. ϕ^0 MESON PRODUCTION

Many of the pions, kaons and protons seen in the spectrometer come from secondary decays rather than from the primary interaction. Very few ϕ^0 mesons, on the other hand, come from secondary decays and so are a good probe of the primary fireball. About 1100 ϕ^0 mesons were found above background.²³ Figure 7(a) shows the resulting ϕ^0 p_\perp distribution. A thermal model distribution with $kT = 0.17\text{GeV}/c$ does not give a good fit. The distribution from the Pythia Monte Carlo does show reasonable agreement. Similarly, in figure 7(b) the dependence of the $\langle p_\perp \rangle$ on multiplicity is flat for both the data and the Pythia Monte Carlo.

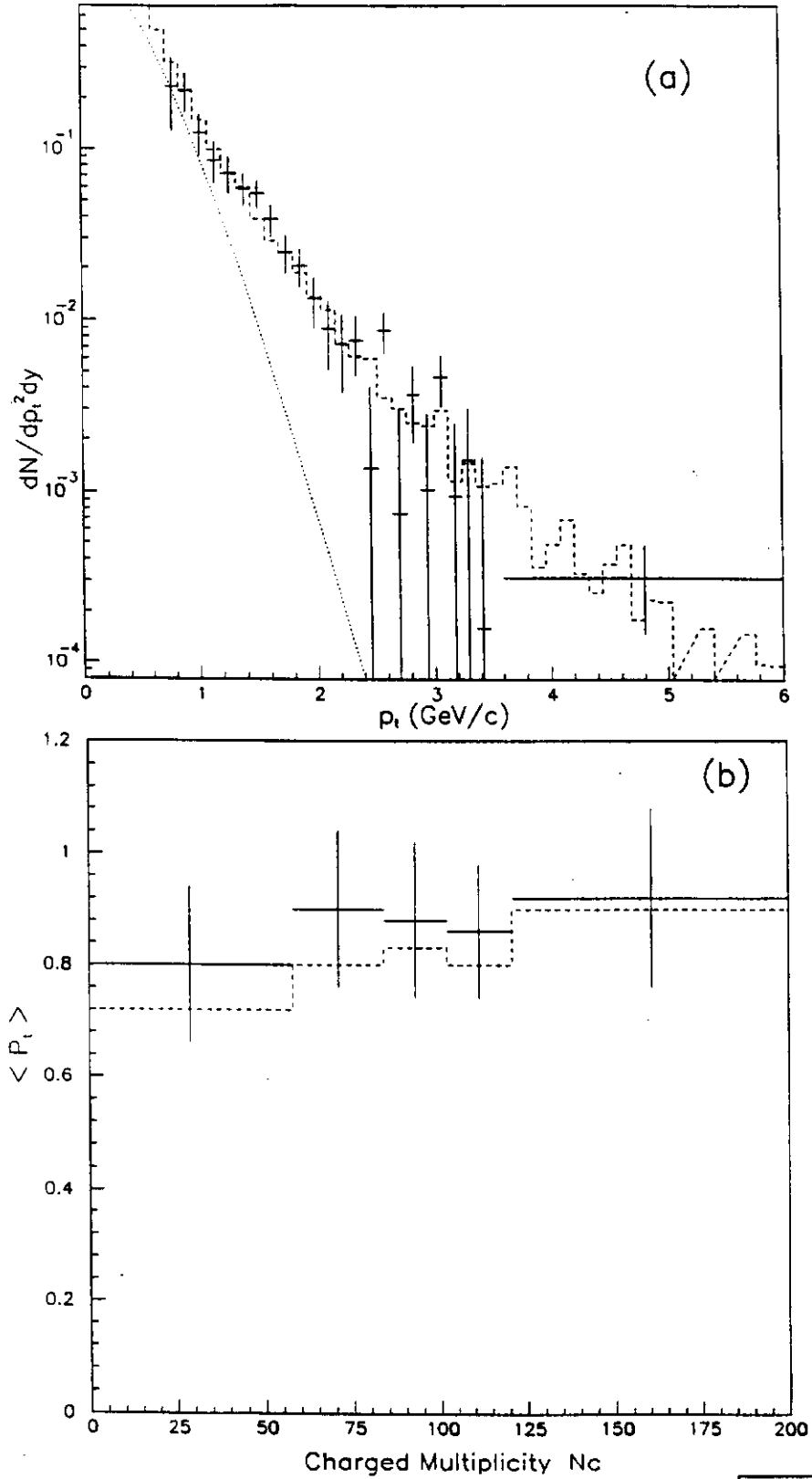


Figure 7. (a) ϕ^0 meson p_{\perp} distribution. Dotted line is fit to $\exp(-\sqrt{p_{\perp}^2 + m^2}/kT)$ where $kT = 0.17$ GeV/c. Dashed histogram is from Pythia Monte Carlo. (b) Average p_{\perp} versus N_c , histogram is from Pythia (ref. 23).

6. BOSE-EINSTEIN CORRELATIONS

With the large statistics available from the second run it became feasible to study two pion Bose-Einstein correlation using the Hanbury-Brown and Twiss technique.²⁴ The two pion correlation was defined as

$$C_2 = \frac{\text{like - charged - pairs - same - event}}{\text{like - charged - pairs - different - events}}$$

and plotted as function of q_\perp or q_0 , where q_\perp is the component of $\vec{q} = \vec{p}_1 - \vec{p}_2$ that is normal to $\vec{p}_1 + \vec{p}_2$ and $q_0 = E_1 - E_2$. Using pions from different events for the denominator helps to produce a correlation free background distribution. Each background pion was combined with a pion from an event with similar event vertex position and multiplicity.

Because of the small spectrometer aperture and the asymmetry of the spectrometer, care must be taken to avoid producing artificial correlations. For example, there were different acceptances for positive and negative charged tracks. This caused different opening angle distributions for $\pi^+\pi^+$, $\pi^-\pi^-$, and $\pi^-\pi^+$ pairs at small angles. Therefore, a minimum opening angle between the two pions of 12° was required. Also, the event vertex distribution of the background pairs was matched to that for signal pairs.

To avoid artificial correlations, three *control* groups were studied: (1) Monte Carlo events with no correlations were put through detector simulation and the resulting events treated with same analysis as real data; (2) Identified πK , πp , and $K p$ same sign pairs from same events and from different events were assigned pion masses and were analyzed in the same way as pion pairs; (3) Opposite sign pions from same and different events ($C_2 = (\pi^+\pi^-)_s / (\pi^+\pi^-)_d$) were analyzed in same way as same sign pairs. None of these three cases showed significant correlations.

Figure 8 shows two pion correlation function versus q_\perp for two multiplicity bins. The distributions were fit to the Gaussian parameterization

$$P = A(1.0 + \lambda \exp -\beta q_\perp^2)$$

where $R = \hbar c \sqrt{\beta}$. Fitting such distributions for several multiplicity bins gave the distributions of R and λ (*chaoticity*) versus multiplicity as shown in figures 9 and 10. The radius increases quite strongly with multiplicity, while the chaoticity decreases. The UA1 data²⁵ at 630 GeV also shows increasing radius with N_c . The difference between the two data in region of $dN/d\eta$ of 5 to 10 is probably due to the more limited phase space selected by the E735 spectrometer and the analysis cuts than to difference in energy. A similar analysis for Gaussian lifetime shows increase from about 0.5 fm to 1.0 fm for $dN/d\eta$ of 7 to 20.

7. Summary

The charged multiplicity of minimum bias $p\bar{p}$ collisions has been measured in three pseudo-rapidity intervals and at four energies, including 1800 GeV. KNO scaling is violated in wide pseudo-rapidity intervals but holds for the most narrow one. A sum of two negative binomials is required to give a good fit to the 1800 GeV full phase space distribution.

Measurements of production of pions, protons, lambdas, cascades and phi mesons have been made, including $\langle p_\perp \rangle$ dependences on multiplicity for all but the cascades.

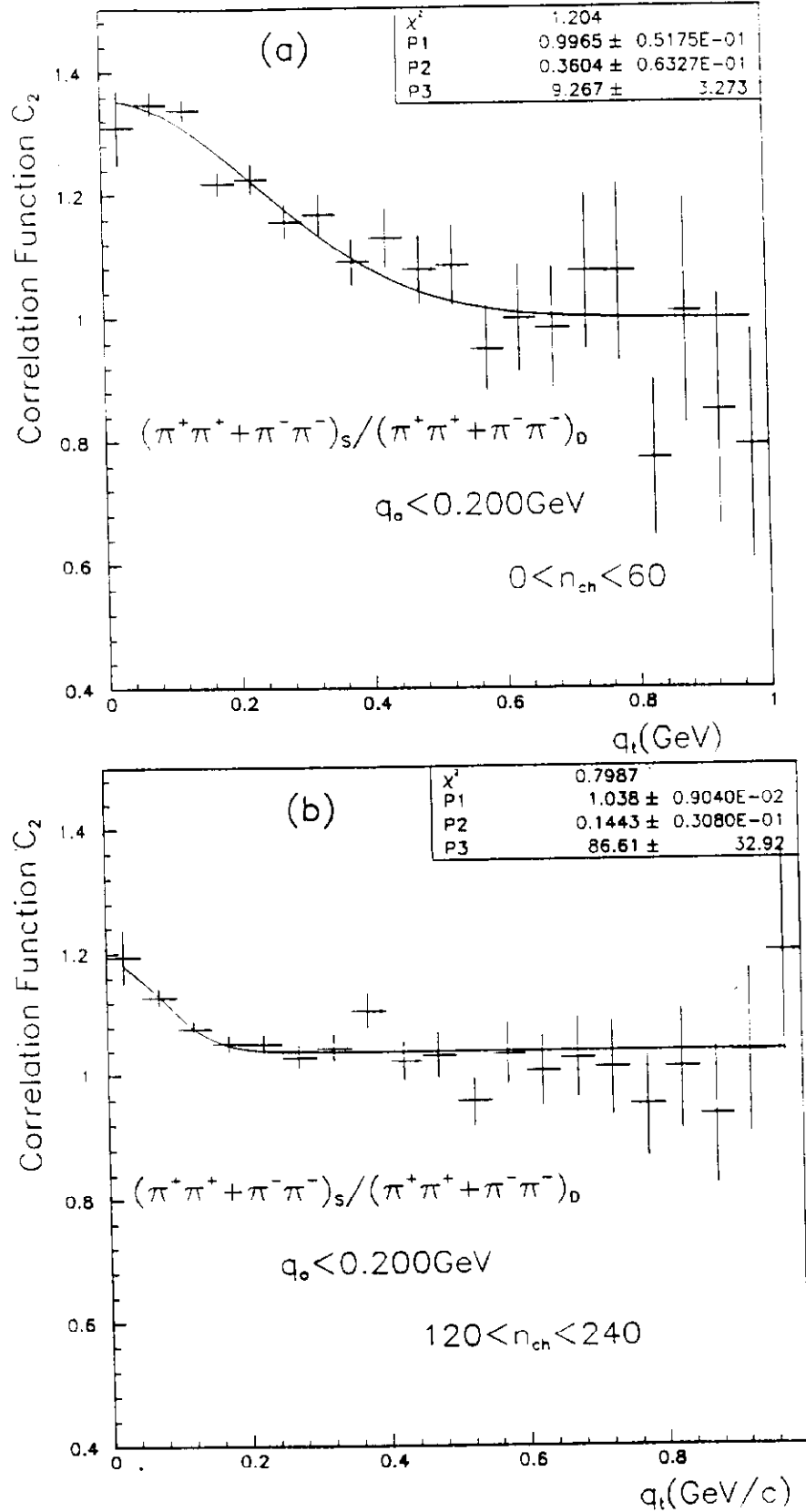


Figure 8. Two pion correlation functions versus q_{\perp} with $q_0 < 0.200 \text{ GeV}/c$ for (a) $0 < N_c < 60$ and (b) $120 < N_c < 240$ (ref. 24).

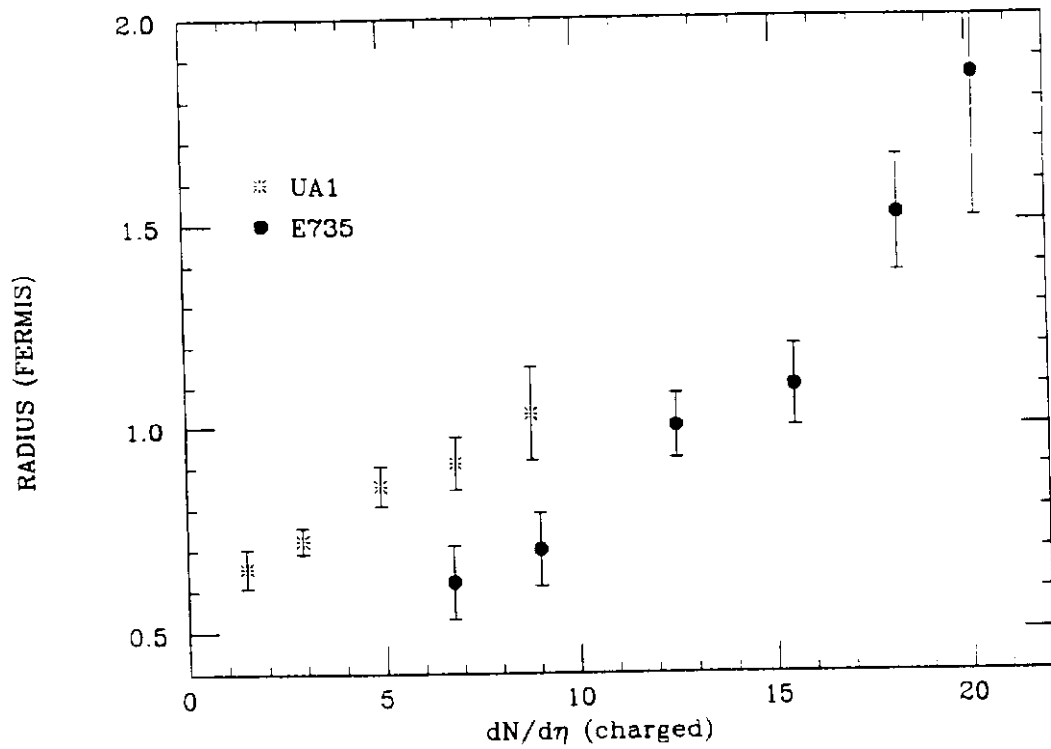


Figure 9. Gaussian radius as function of multiplicity (ref. 24).

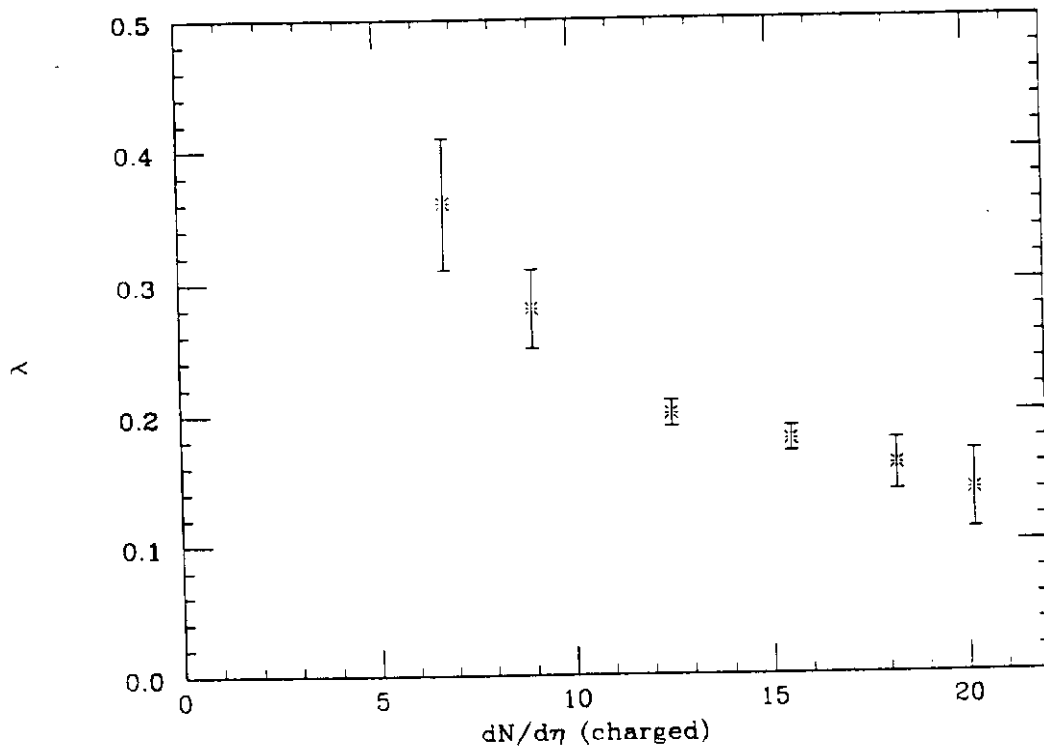


Figure 10. Chaoticity as function of multiplicity (ref. 24).

The proton and lambda $\langle p_{\perp} \rangle$ increases with multiplicity, whereas the phi $\langle p_{\perp} \rangle$ is flat. The lambda to proton ratio is flat as function of multiplicity.

Bose-Einstein correlations for two pions indicate an increasing radius and lifetime with increasing multiplicity. The chaoticity decreases with multiplicity.

None of these or previous E735 results give unambiguous signals for QGP formation. For example, one model has shown that the E735 $\langle p_{\perp} \rangle$ vs N_c dependencies for pion, kaon, proton and lambda are consistent with transverse flow in a plasma.²⁶ However, a mini-jet model has also been shown to be consistent with these $\langle p_{\perp} \rangle$ distributions.²⁷ Regardless of whether any clear QGP signal is found, we believe the E735 results place important constraints on any model of soft p_t proton-antiproton physics.

References

1. D. Bjorken, Phys. Rev. D. 27 (1983) 140.
2. L. Van Hove, Phys. Lett. 118B, 138 (1982).
3. T. Alexopoulos et al. (E735 Collaboration), Phys. Rev. Lett. 60 (1988) 1622.
4. S. Banerjee et al. (E735 Collaboration), Phys. Rev. Lett. 62 (1989) 12.
5. T. Alexopoulos et al. (E735 Collaboration), Phys. Rev. Lett. 64 (1990) 991.
6. F. Turkot et al. (E735 Collaboration), Nucl. Physics A525 (1991) 165c-170c.
7. C. Findeisen et al., Submitted to Nucl. Instrum. and Methods.
8. C. Allen et al., Nucl. Instrum. and Methods. A294 (1990) 108.
9. E.W. Anderson et al., Nucl. Instrum. and Methods. A295 (1990) 86.
10. S. Banerjee et al., Nucl. Instrum. and Methods. 269A (1988) 121.
11. Hojvat et al., to be submitted to Nucl. Instrum. and Methods.
12. S. Oh et al., Nucl. Instrum. and Methods. A303 (1991) 277.
13. G.J. Alner et al. (UA5 Collaboration), Nucl. Physics B291 (1987) 445-502.
14. T. Sjöstrand and M. van Wijn, Phys. Rev. D36 (1987) 2019.
15. CERN, Geant3 Users Guide, CERN DD/EE/84-1 (1985).
16. C. Fuglesang, Nucl. Instrum. and Methods. A278 (1989) 765-773.
17. G. J. Alner et al. (UA5 Collaboration), Phys. Rep. 154 (1987) 247.
18. R. E. Ansorge et al. (UA5 Collaboration), Z. Phys. C 43 (1989) 357.
19. C. Albajar et al. (UA1 Collaboration), Nucl. Phys. B335 (1990) 261.
20. C. Fuglesang, "UA5 Multiplicity Distributions and Fits of Various Functions", Proc. of Multiparticle Dynamics Conf., La Thuile, Italy, March 1989.
21. C. H. Wang, "Multiplicity Distributions of Charged Particle Secondaries from Proton-Antiproton Collisions at the Tevatron Collider $\sqrt{s} = 1.8\text{TeV}$ ", submitted to the Proc. of Particles and Fields Conf., 1991, Vancouver, B.C.
22. Alexopoulos et al. (E735 Collaboration), "Hyperon Production from Proton-Antiproton Collisions at $\sqrt{s} = 1.8\text{TeV}$ ", DUKHEP91-10, submitted Phys. Rev. D.
23. J. Jennings, " ϕ^0 Meson Production in $p\bar{p}$ Collisions at the Tevatron Collider at $\sqrt{s} = 1.8\text{TeV}$ ", submitted to the Proc. of Particles and Fields Conf., 1991, Vancouver, B.C.
24. T. Alexopoulos, "A Measurement of the Bose-Einstein Correlation for Two Pions in Proton-Antiproton Collisions at Center of Mass Energy 1.8TeV", Ph.D. thesis, Univ. of Wisconsin, Madison (1991).
25. J.D. Dowell from UA1 Collaboration, Proc. of the VII Topical Workshop on Proton-Antiproton Collider Physics, p.115, World Scientific 1989.
26. P. Lévai & B. Müller, Phys.Rev.Lett. 67(1991)1519. Also see Müller this proceedings.
27. X. Wang and M. Gyulassy, "A Systematic Study of Particle Production in $p + p(\bar{p})$ Collisions via the HIJING Model", preprint LBL-31159.